Proceedings of OMAE 2004
23rd International Conference on Offshore Mechanics and Arctic Engineering
20-25 June 2004 Vancouver

OMAE2004-51085

THE NUMERICAL SIMULATION OF LNG SLOSHING WITH AN IMPROVED VOLUME OF FLUID METHOD

Erwin Loots

MARIN
PO Box 28
6700 AA Wageningen
The Netherlands

Wouter Pastoor

DNV
Veritasveien 1
1322 Høvik
Norway

Bas Buchner

MARIN
PO Box 28
6700 AA Wageningen
The Netherlands

Trym Tveitnes

DNV
Veritasveien 1
1322 Høvik
Norway

ABSTRACT

With the trend towards offshore LNG production and offloading, sloshing of LNG in partially filled tanks has become an important research subject for the offshore industry. LNG sloshing can induce impact pressures on the containment system and can affect the motions of the LNG carrier.

So far, LNG sloshing was mainly studied using model tests with an oscillation tank. However, the development of Navier-Stokes solvers with a detailed handling of the free surface, nowadays allows the numerical simulation of sloshing. It should be investigated, however, how accurate the results of this type of simulations are for this complex flow problem.

The present paper first presents the details of a numerical model, an improved Volume OF Fluid (iVOF) method. Comparisons are made with sloshing model test results. Based on the results, the following conclusions can be drawn:

- The dynamics of sloshing in LNG tanks can be simulated numerically using an iVOF Navier-Stokes solver.
- Several improvements have been made in the treatment of numerical spikes in the pressure signals, but still more improvements need to be made.
- Qualitatively, the pressure pulses resulting from impacts against the LNG tank wall show a rather good agreement between experiment and numerical simulation.
- Quantitatively, the differences with the experiment show that further detailed studies with respect to cell sizes and time steps are necessary.

INTRODUCTION

Seaborne LNG transportation has up until now primarily involved ships sailing on long term contracts with full tanks on the laden voyage and almost empty tanks on the ballast voyage. The current trend towards offshore LNG production and offshore discharge from LNG carriers may impose a challenge with respect to sloshing induced loads on the tank containment system, as such operation will involve intermediate filling of the cargo tanks when at sea.

So far sloshing loads have mainly been determined through model testing. Model testing is expensive and time consuming and not practical in a design loop (e.g. for tank shape optimization aiming to reduce sloshing loads). Therefore, a numerical tool that allows simulation of liquid motion inside slack LNG tanks and calculation of pressure loading on the tank boundaries are of great value, both as a design tool for relative evaluation of two designs and as a tool for predicting absolute values of pressure loading on the LNG tank containment system. In the present paper a numerical model for simulation of sloshing is presented together with an example of application for calculation of sloshing induced loads on a membrane type LNG cargo tank. The latter also includes a comparison with experimentally obtained sloshing loads.

In the paper first the details of the numerical model, an improved Volume OF Fluid (iVOF) method are presented. The program has been developed initially to study the sloshing of liquid fuel in satellites. This micro-gravity environment

requires a very accurate and robust description of the free surface. Coupled dynamics between the sloshing fluid and the satellite were investigated as well [Ref. 1,2]. Later, this methodology was later extended to the calculation of green water loading on a fixed bow deck [Ref.3, 5] and the analysis of anti-roll tanks, including the coupling with ship motions [Ref. 4]. Finally the entry of a wedge in a fluid was studied [Ref. 7].

Thereafter, results of LNG sloshing simulations will be presented and discussed. Comparisons will be made with sloshing model test results. Aspects like impact pressure accuracy, pressure pulse durations and mesh size are discussed in the paper.

THE NUMERICAL MODEL

ComFLOW is an improved 3D Volume Of Fluid (iVOF) Navier-Stokes solver. The program has been developed initially by the University of Groningen/RuG (Prof.dr. Arthur Veldman) to study the sloshing of liquid fuel in satellites. This micro-gravity environment requires a very accurate and robust description of the free surface. Coupled dynamics between the sloshing fluid and the satellite were investigated as well (References [1] and [2]). In close co-operation with MARIN, this methodology was later extended to the calculation of green water loading on a fixed bow deck (Reference [3]). Also anti-roll tanks, including the coupling with ship motions (Reference [4]), were investigated. Furthermore, the entry of a wedge in a fluid was studied as part of the RuG-MARIN co-operation (Reference [7]), as well as the wave impact loads on fixed structures (see Figure 1) . Recently, the wave run-up on a GBS was studied (Reference [8]).

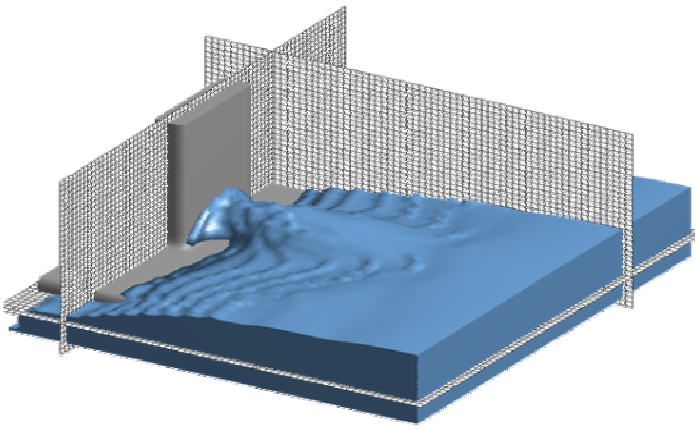

Figure 1: Wave impact simulation; the 3D grid is also shown.

The Volume Of Fluid (VOF) algorithm as developed by Hirt and Nichols (see Reference [9]) is used as a basis for the fluid advection. The method solves the incompressible Navier-Stokes equations with a free-surface condition on the free boundary. In the VOF method a VOF function F (with values between 0 and 1) is used, indicating which part of the cell is filled with fluid. The VOF method reconstructs the free surface in each computational cell. This makes it suitable for the prediction of all phases of the local free surface problem.

First the mathematical and numerical model will be summarised. This will be limited to the main aspects, because the detailed numerical aspects are outside the scope of the present paper. Excellent overviews of the numerical details of the method can be found in References [1] through [4]. To distinguish between the original VOF method of Hirt and Nichols (1981) and the present method with its extensive number of modifications, the name improved-VOF (iVOF) method will be used in the rest of this paper.

Mathematical model

The incompressible Navier-Stokes equations describe the motions of a fluid in general terms. They are based on conservation of mass (Expression 1) and momentum (Expressions 2 through 4).

$$\frac{\partial u}{\partial x}+\frac{\partial v}{\partial y}+\frac{\partial w}{\partial z}=0 \qquad (1)$$

$$\frac{\partial u}{\partial t}+u\frac{\partial u}{\partial x}+v\frac{\partial u}{\partial y}+w\frac{\partial u}{\partial z}=-\frac{1}{\rho}\frac{\partial p}{\partial x}+\nu\left(\frac{\partial^2 u}{\partial x^2}+\frac{\partial^2 u}{\partial y^2}+\frac{\partial^2 u}{\partial z^2}\right)+F_x \qquad (2)$$

$$\frac{\partial v}{\partial t}+u\frac{\partial v}{\partial x}+v\frac{\partial v}{\partial y}+w\frac{\partial v}{\partial z}=-\frac{1}{\rho}\frac{\partial p}{\partial y}+\nu\left(\frac{\partial^2 v}{\partial x^2}+\frac{\partial^2 v}{\partial y^2}+\frac{\partial^2 v}{\partial z^2}\right)+F_y \qquad (3)$$

$$\frac{\partial w}{\partial t}+u\frac{\partial w}{\partial x}+v\frac{\partial w}{\partial y}+w\frac{\partial w}{\partial z}=-\frac{1}{\rho}\frac{\partial p}{\partial z}+\nu\left(\frac{\partial^2 z}{\partial x^2}+\frac{\partial^2 z}{\partial y^2}+\frac{\partial^2 z}{\partial z^2}\right)+F_z \qquad (4)$$

$\vec{F}=(F_x, F_y, F_z)$ is an external body force, such as gravity.

With:

p	=	pressure
t	=	time
u	=	velocity in x-direction
v	=	velocity in y-direction
w	=	velocity in z-direction
x	=	x-position
y	=	y-position
z	=	z-position
ν	=	kinematic viscosity
ρ	=	fluid density

The Navier-Stokes equations can also be written in a shorter notation as:

$$\nabla\cdot\vec{u}=0 \qquad (5)$$

$$\frac{\partial\vec{u}}{\partial t}+\nabla p=\vec{R} \qquad (6)$$

$\vec{R}$ now contains all convective, diffusive and body forces.

Numerical model: geometry and free surface description

For the discretisation of a computational domain in numerical simulations a large number of different methods are available. Basically, they can be divided into:

- Structured and unstructured grids
- Boundary fitted and non-boundary fitted grids

In the improved-VOF method a structured (Cartesian) non-boundary fitted grid (not necessarily equidistant) is chosen. This has the following advantages related to the use of the method for the prediction of wave loading:

- Easy generation of the grid around complex structures
- A lot of research on surface tracking on orthogonal grids has been carried out
- Moving objects in the fluid can be dealt with in a similar way as fixed boundaries, without re-gridding

The main disadvantage of this discretisation method is the fact that the boundary and free surface are generally not aligned with the gridlines. This requires special attention in the solution method, as will be shown below.

An indicator function is used in the form of volume and edge apertures to track the amount of flow in a cell and through a cell face:

- Volume aperture: the geometry aperture F_b indicates which fraction of a cell is allowed to contain fluid ($0 \le F_b \le 1$). For bodies moving through the fluid, the geometry aperture may vary in time. The time-dependent fluid aperture F_s indicates which fraction of a cell is actually occupied by fluid and satisfies the relation $0 \le F_s \le F_b$.
- Edge aperture: the edge apertures A_x, A_y, and A_z define the fraction of a cell surface through which fluid may flow in the x, y and z direction respectively. Obviously, these apertures are between zero and one.

Figure 2 shows a two-dimensional example with $F_b = 0.8$ and $F_s = 0.3$.

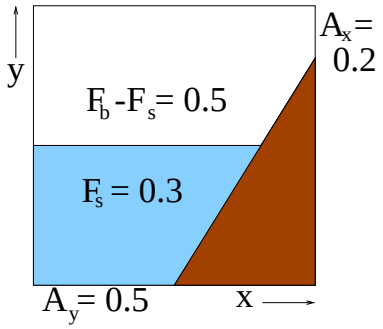

Figure 2: Two-dimensional example of a grid cell using apertures

After the apertures have been assigned to the grid cells and the cell edges, every cell is given a label to distinguish between boundary, air and fluid. Two classes of labelling exist: Geometry cell labels and fluid cell labels. The geometry labelling at each time step divides the cells into three classes:

F(low)-cells : All cells with $F_b \ge 0$

B(oundary)-cells : All cells adjacent to a **F**-cell

(e)**X**(ternal)-cells : All remaining cells

The free-surface cell labelling is a subdivision of the **F**-cells. The subdivision consists of 3 subclasses:

E(mpty) cells : All cells with $F_s = 0$

S(urface) cells : All cells adjacent to an **E**-cell

F'(luid)-cells : All remaining **F**-cells

Figure 3 shows an example of geometry cell labelling and free-surface cell labelling for a wedge entering a fluid.

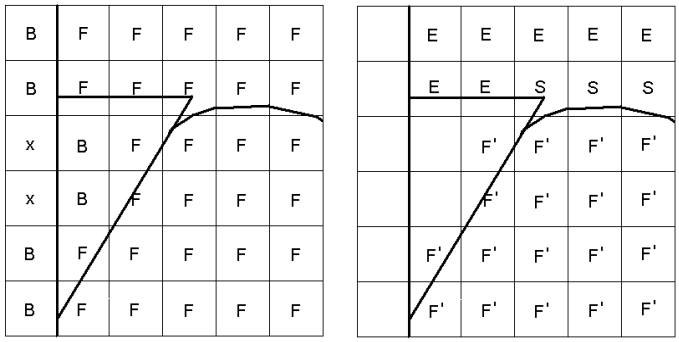

Figure 3: Geometry cell labelling (left) and free-surface cell label for a wedge entering a fluid (right)

The discretisation of the Navier-Stokes equations is done on a staggered grid, which means that the pressure will be set in the cell centres and the velocity components in the middle of the cell faces between two cells. This is shown in 2D in Figure 4.

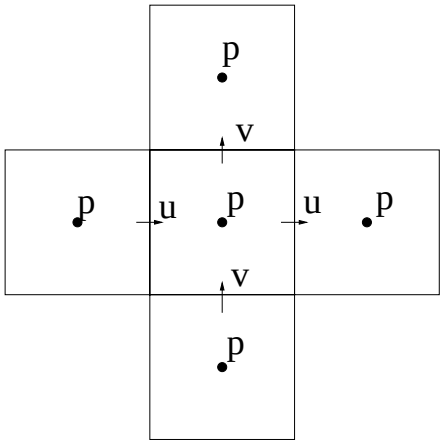

Figure 4: Location of the pressure and velocity components in the staggered grid

The Navier-Stokes equations, as given by Eqns. (5) and (6), are discretised in time according to the explicit first order Forward Euler method as follows:

$$\nabla.\vec{u}^{n+1} = 0 \tag{7}$$

$$\frac{\vec{u}^{n+1} - \vec{u}^{n}}{\Delta t} + \nabla p^{n+1} = \vec{R}^{n} \tag{8}$$

Δt is the time step and n+1 and n denote the new and old time level, respectively. The conservation of mass in Expression (7) and the pressure in Expression (8) are treated on the new time level n+1 to assure that the new $\vec{u}$ is divergence-free (no gain or loss of fluid).

The spatial discretisation will now be explained using the computational cell shown in Figure 5.

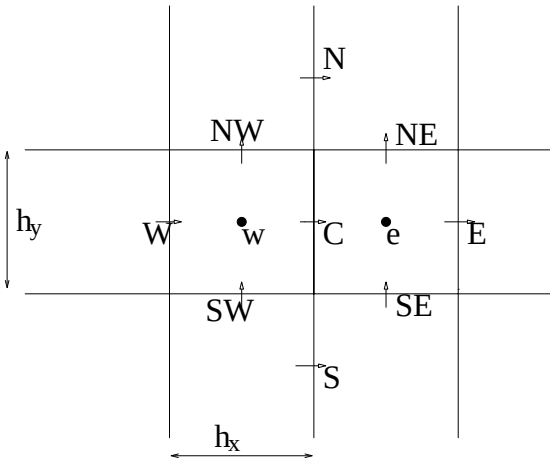

Figure 5: Spatial discretisation cell, using compass indication for cell phases

Expression (7) is applied in the centres of the cells and a central discretisation is used. In the cell with centre w the discretised equation becomes:

$$\frac{u_C^{n+1} - u_W^{n+1}}{h_x} + \frac{v_{NW}^{n+1} - v_{SW}^{n+1}}{h_y} = 0 \tag{9}$$

The momentum Expression (8) is applied in the centres of the cell faces, thus the discretisation in point C becomes:

$$\frac{u_C^{n+1} - u_C^{n}}{\Delta t} + \frac{p_e^{n+1} - p_w^{n+1}}{h_x} = R_C^{n} \tag{10}$$

In the detailed work of Gerrits (Reference [2]) other aspects of the numerical method are described in detail, such as:

- Discretisation of R_c^n
- Discretisation near the free-surface
- In- and outflow discretisation
- Pressure Poisson equation
- Free surface reconstruction and displacement
- Use of the Courant-Friedrichs-Levy (CFL) number
- Calculation of forces

The following functionalities are presently available in ComFLOW :

- Calculation of the fluid motion by solving the incompressible Navier-Stokes equations.
- One type of fluid flow is considered, with a void where no fluid is present.
- Possibility to model an arbitrary number of fixed objects in the fluid. The objects are defined piecewise linearly.
- Options to use no-slip or free-slip boundary conditions at the solid boundaries. At the free surface continuity of tangential and normal stresses (including capillary effects) is prescribed. Inflow and outflow boundary conditions for fluid velocities and/or pressures can be defined.
- The fluid simulations are carried out on a Cartesian grid with user-defined stretching. The Cartesian grid is fixed in the domain. When the domain is moving a virtual body force is added to the forcing term in the Navier-Stokes equations. The fluid motions are thus solved in a domain-fixed co-ordinate system.
- To distinguish between the different characters of grid cells, the cells are labelled. The Navier-Stokes equations are discretized and solved in cells that contain fluid. The free-surface displacement is described by the Volume Of Fluid method with a local height function.

Numerical model: free surface velocities and pressure spikes

In a typical sloshing simulation, the configuration of the free surface will often change quite rapidly. Moreover, a lot of topological changes will occur. Therefore, it is very important to describe the velocities properly. Consider the situation in Figure 6.

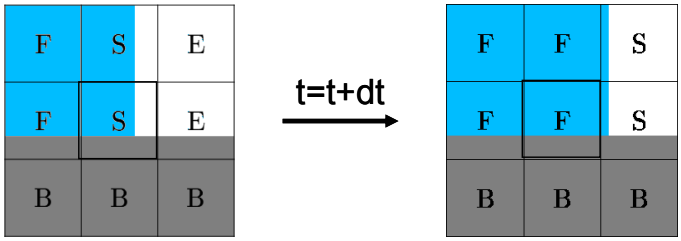

Figure 6: Motion of free surface changes the labelling.

The S-E velocity at the old time step changes to an F-S velocity at the new time step. The S-E velocity was set by using a boundary condition for the free surface. If this is not properly done, the pressure has to 'work' to achieve mass conservation in the newly created F cell. This 'work' will manifest itself in a spike in the pressure signal, see the left-hand picture of Figure 7. When proper boundary conditions at the free surface are chosen (see below), the signal becomes smoother (right-hand picture). Note that, especially in 3D, a lot of free surface configurations near solid boundaries occur which have to be taken care of. Especially when large amounts of fluid smash against a wall or when air bubbles collapse, pressure spikes can not always be prevented [Ref. 6].

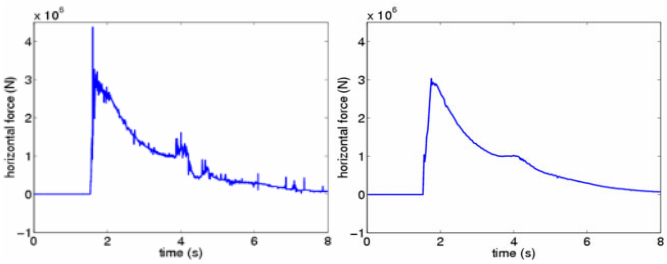

Figure 7: Pressure signals before (left) and after (right) properly accounting for mass conservation in cut cells.

Consider for example the situation in Figure 8. This is a situation that could typically happen in the LNG tank. The water front moves from the old time step (left) to the configuration shown in the right-hand picture. The bold lined E cell becomes an F cell in a single time step. In E cells no conditions are satisfied with respect to mass conservation, so the sudden demand for divergence free velocities in the newly created F cell cannot be met without the above mentioned action by the pressure field: a spike.

To resolve this, E-F transitions can be detected in the process. When such a transition has occurred, we can look for an F-S velocity (in this case, the velocity between the two bold lined cells in the right-hand picture) and adjust this velocity such that mass conservation holds in the new F cell. Such an F-S velocity can almost always be found when the free surface moves perpendicular to a wall.

However, when smashing occurs, as in some cases in the LNG tank simulations, no F-S velocities will be available. The pressure spike can not be prevented in those configurations, which is in some sense is according to the physics (see Figure 9).

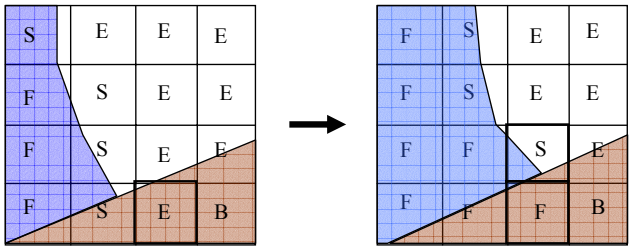

Figure 8: Situation of label changes: a small E cell becomes an F cell.

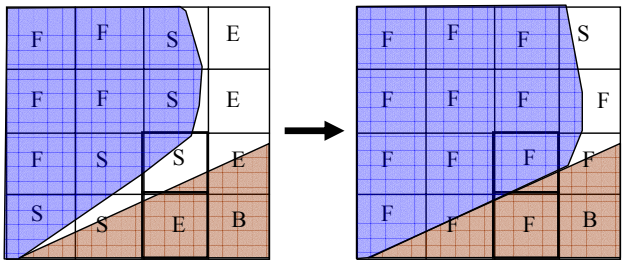

Figure 9: A free surface smashes against a wall. The E cell in the left picture becomes an F cell in the next time step (right picture). No F-S velocities are present to repair the conservation of mass. A pressure spike will occur.

Numerical model: motions

An important feature of the method is that the geometry does not move; that means that the geometrical information, i.e. the geometry apertures F_b and A_x, A_y, and A_z, as defined at the start of the simulation stay the same. (Prescribed) motions of the geometry, like the movement of the LNG tank, are dealt with using reference frames and virtual body forces**.**

The inertial reference frame is called O_i and in this reference system the gravity is directed downwards. This is the situation at the start of the simulation. The geometry reference frame O_g , in which all equations are discretised, moves with respect to the former.

That means that the gravity vector will change during the simulation. The two coordinate systems are related by the unity vectors

$$\vec{d}_i \text{ such that } O_g = \left(\vec{d}_1 \quad \vec{d}_2 \quad \vec{d}_3\right) O_i .$$

The momentum equations (2) -- (4) are extended to:

$$\frac{D\vec{u}}{Dt} = -\frac{1}{\rho}(\nabla p - (\nabla.\mu\nabla)\vec{u}) + \vec{F} + \vec{f} \qquad (11)$$

where $\vec{f}$ is given by:

$$\vec{f} = -\vec{q} - \frac{d\vec{\omega}}{dt} \times \vec{r} - \vec{\omega} \times (\vec{\omega} \times \vec{r}) - 2\vec{\omega} \times \vec{u} \qquad (12)$$

with:

- $\vec{q}$ the acceleration of the moving system O_g with respect to O_i;
- $\vec{\omega}$ the angular velocity vector of the moving system O_g with respect to O_i
- $\vec{r}$ is the position of the liquid particle in O_g.

Using Newton's third law, this extra term $\vec{f}$ in equation (11) can be seen as an acceleration due to a virtual body force: instead of actually moving the solid body in the numerical model, the fluid is subjected to an acceleration (equal in magnitude and opposite in sign) to account for the solid-body motion.

For the application of the moving LNG tank, the time series of linear motion (surge, sway, heave) and their 2nd order derivatives in time have to be translated to $\vec{q}$, while the three angular motions (roll, pitch, yaw) and their derivatives will provide the angular rotation vector $\vec{\omega}$ and its derivative.

Further, the gravity vector has to be adjusted with respect the unit vectors, in the opposite direction:

$$g_g = \left(\vec{d}_1 \quad \vec{d}_2 \quad \vec{d}_3\right)^{-1} g_i$$

To summarize, the proper application of these formulas boils down to straightforward linear algebra and the bookkeeping of the transformation matrices. The computational geometry does not have to change. The motion of the geometry becomes merely a post-processing task.

MODEL TESTS

For the purpose of obtaining experimental data to compare sloshing loads calculated by ComFLOW, a sloshing experiment with a 1/20 scale model of a conventional size membrane type LNG carrier cargo tank was set up (Figure 10, Figure 11).

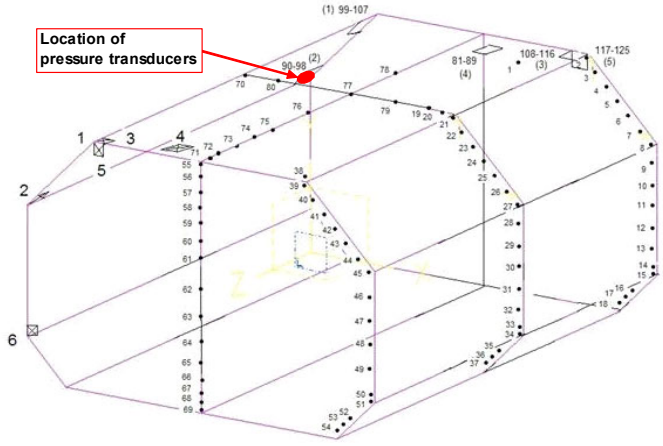

Figure 10: Drawing of the LNG tank model. Note the location of the pressure sensors in the corner

Figure 11: The LNG tank model

The tank model was excited with a regular sway motion at a frequency close to the natural period of the liquid for the particular filling height that was used. The filling was 70% of the tank height. The excitation period was 1.7 seconds and the amplitude of sway was 0.06 meters.

It should be noted that this case is a first case to check the iVOF method. It does not represent yet the high impact peaks, or short rise times, that are expected as the worst cases in LNG tanks.

The sloshing induced pressure loading on the lower knuckle of the upper chamfer in way of the forward tank end was measured using a cluster of 9 pressure transducers within an area of 6 by 6 cm. The sensor readings were averaged to represent the time history of pressure over 6 by 6 cm. The location of the sensors is indicated in Figure 11.

The duration of the test was about 30 minutes, yielding more than 1000 cycles or sloshing pressure pulses. Results of twenty of such pulses are shown in Figure 12. They are used in combination with the numerical simulations in the remainder of this paper.

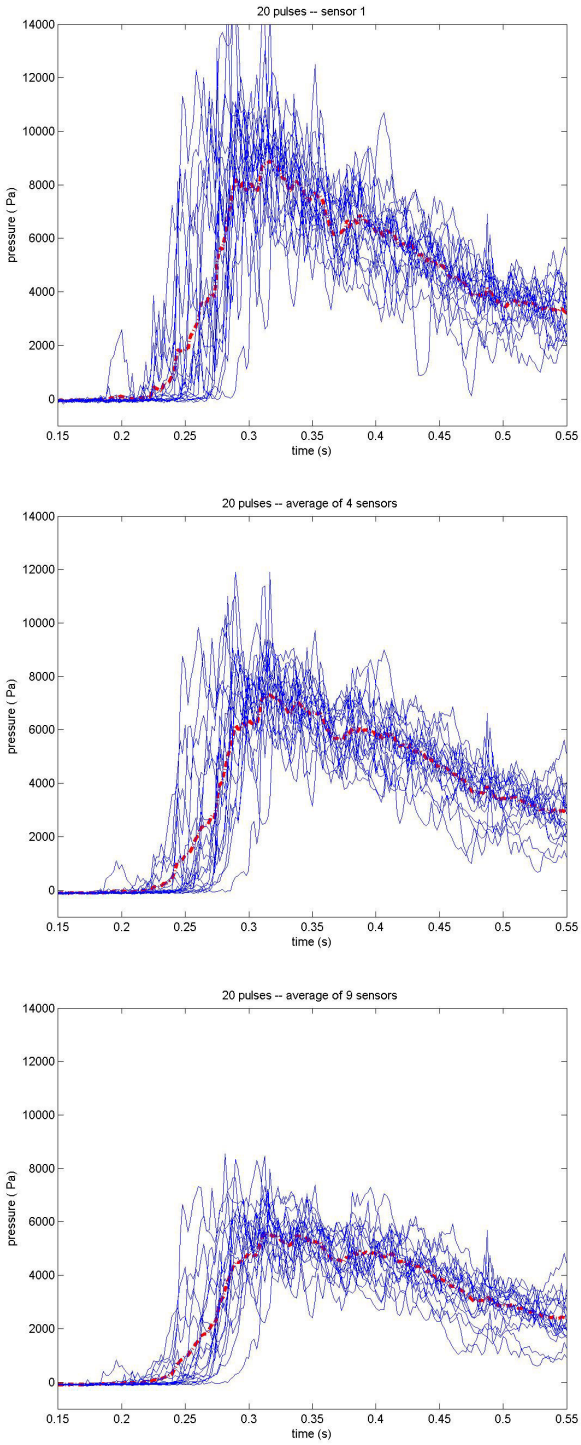

Figure 12: Comparison of twenty pulses from the experiment: one sensor (1st figure), averaged over 4 sensors (2nd figure), averaged over all 9 sensors (3rd figure).

NUMERICAL SIMULATIONS

After that, the experiment was simulated numerically with ComFLOW. Several grids were chosen, and the time step was also varied, see Table 1. The coarsest grid has cell sizes of exactly 6x6 cm: the size of the cluster that included 9 pressure transducers. All simulations lasted twenty periods (34 s). It turned out that the situation described in Figure 9 happened rather often, hence the high number of pressure spikes.

Table 1 Performed simulations

Grid	Time step (s)	Pressure maximum (kPa)		Mean rise time (s)
		original	filtered	
31x24	0.01	5.1	4.4	0.088
31x24	0.005	6.4	4.1	0.085
31x24	0.0025	8.8	4.3	0.084
31x24	0.00125	11.4	4.1	0.088
62x48	0.005	9.0	7.6	0.048
62x48	0.0025	11.8	6.6	0.065
62x48	0.00125	10.4	5.4	0.063
124x96	0.00125	8.5	6.5	0.054
124x96	0.000625	10.5	5.5	0.041

These numerical spikes all have a duration of a single time step. The locations and heights are very dependent on the grid size and the time step. The signals were filtered in order to apply statistics like the determination of the rise time. The filtered value at each time step is defined as the minimum of two consecutive values: $p_i^{new} = MIN(p_i^{old}, p_{i+1}^{old})$. The effect is seen in Figure 13.

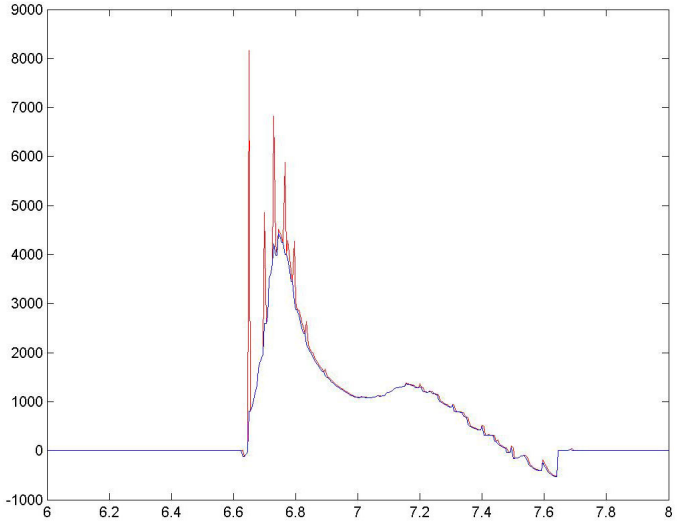

Figure 13: Effect of the filter to avoid numerical spikes.

As can be seen in Table 1, the average of the 20 unfiltered peak heights increases both when we decrease the time step and when we decrease the grid size.

The left-hand figure of Figure 14 shows that the pulses on the coarsest grid are rather consistent. The rise time is long. Simulations on the finer grids show more variation in start times and shape of the pulses. The coarsest grid seems unable to capture the physical details needed for these kind of sloshing problems. On the other hand, variations on the finer grids are highly dependent on time steps and grid sizes, which at least indicates that the physical aspects involved are far from trivial.

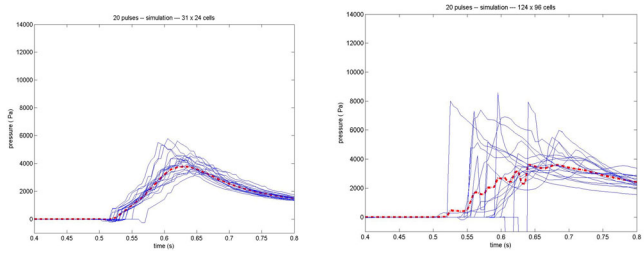

Figure 14: twenty pulses shown for simulations on a coarse grid of 31x24 cells (first figure), and on a fine grid of 124x96 cells (2nd figure).

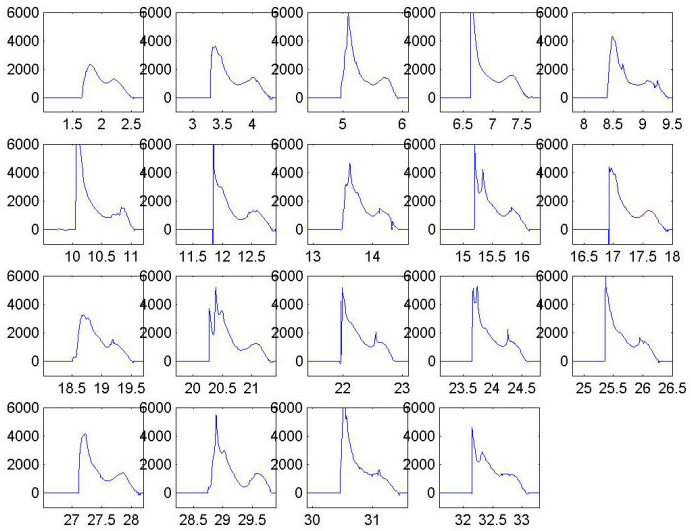

Figure 15: pressure pulses (filtered) in the 124x96 cells simulation

The main observation is that the slope of the pressure pulse varies significantly in duration as well as in height. This holds for both the experiment (Figure 12) and the numerical simulations (Figure 15 and right-hand picture of Figure 14). Globally, the pressure pulses seem to appear in two kinds. If we take a closer look at these two variants (Figure 16), the rise time of the left-hand pulse (A) is considerably higher than in the right-hand pulse (B), where the pulse is almost instantaneously. The latter kind of pulse appears more often in the simulations with finer grids and smaller time steps; hence the larger rise time in the first four simulations.

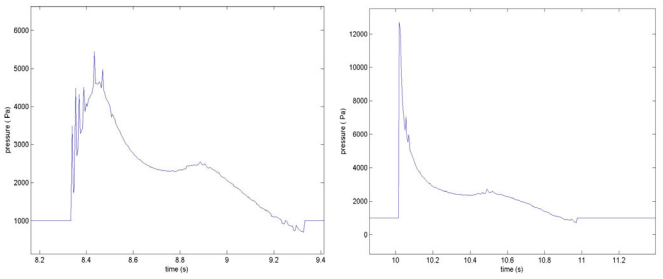

A B

Figure 16: Two typical pressure pulses: long rise time (A) and short rise time (B).

If we look at the details of the free surface, we see that this phenomenon is related to the presence or absence of a bore at the moment of impact in the corner. If the bore moving towards the left meets the upward moving fluid at the right moment, a pulse with a steep slope will appear, see Figure 18. The snapshots are colored by the horizontal velocity. The bore is identified with the deep blue area at the free surface. Otherwise, if the bore is too late or does not exist, the pulse is dominated by the impact of the upward moving fluid, resulting in a more transient behaviour: Figure 17.

Concerning the remainder of the pulse, we see in Figure 15 that the second maximum is very consistent in the numerical simulations: it appears 0.55 s after the start at the pulse and has a value of approximately 0.0135 bar. It is caused by the fluid falling down again along the wall.

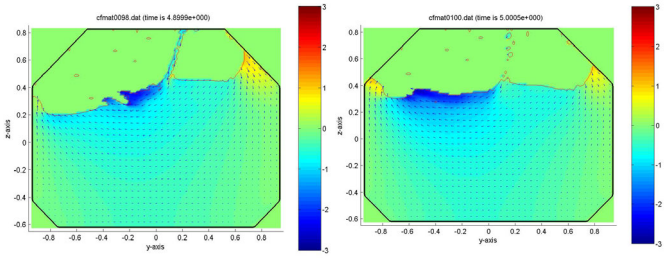

Figure 17: fluid configurations before and after pressure peak A

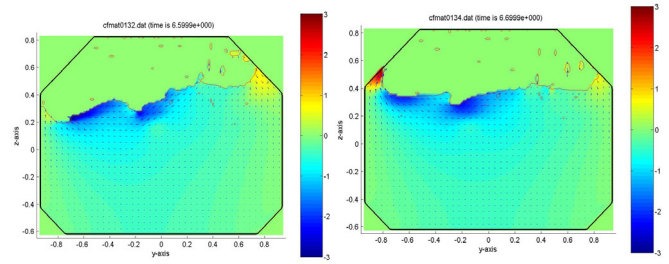

Figure 18: fluid configurations before and after pressure peak B

From the experiments (Figure 12) it is clear that the pressure peak is rather local. The pressure was evaluated at different areas to investigate this. The most local pressure is measured by sensor 1, in the corner. This sensor measures the highest values while the averaged pulses over 2x2 sensors (2nd figure) and over all 3x3 sensors (3rd figure) are considerably lower. This phenomenon is also observed in the numerical simulations. Because they are 2D, we have to compare the pressures along a line (line segment AB, see Figure 19). The first part of this line covers the area where the sensor cluster in the experiment is located. A similar decay in pressure from A towards B (halfway the wall) is observed (see Figure 20), albeit not as large as in the experiment.

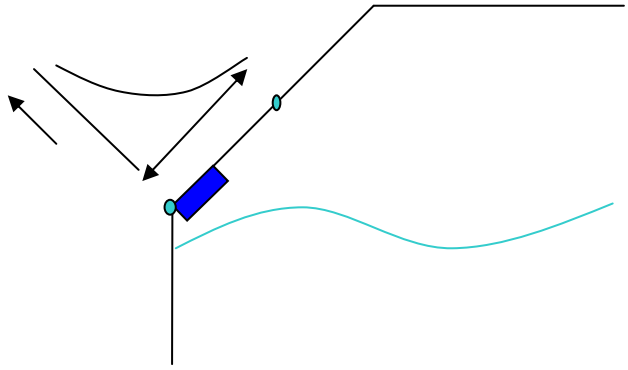

Figure 19: Typical variation of the averaged pressure along the wall

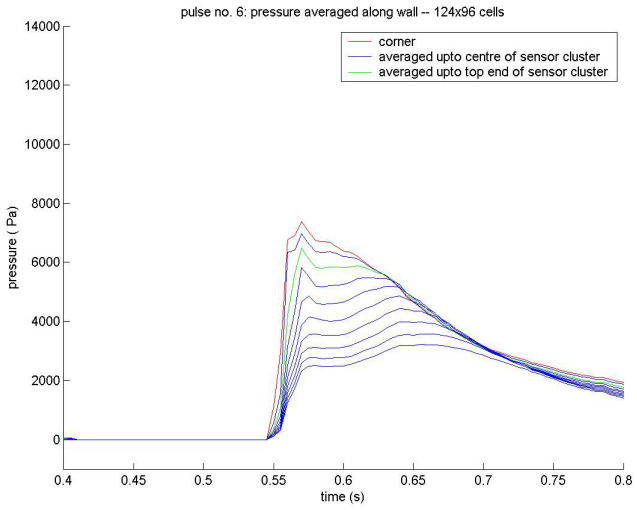

Figure 20: Effect of the area where the peak pressure is measured: averaged pressure from points A to B of a typical pulse. The first three lines are inside the sensor cluster.

CONCLUSIONS

Based on the results presented in this paper, the following conclusions seem justified:

- The dynamics of sloshing in LNG tanks can be simulated numerically using an iVOF Navier-Stokes solver.
- Several improvements have been made in the treatment of numerical spikes in the pressure signals, but still more improvements need to be made.

- Qualitatively, the pressure pulses resulting from impacts against the LNG tank wall show a rather good agreement between experiment and numerical simulation.
- Quantitatively, the differences with the experiment show that further detailed studies with respect to cell sizes and time steps are necessary.

REFERENCES

1. Gerrits, J., Loots, G.E., Fekken, G. and Veldman, A.E.P.: 1999, Liquid Sloshing on Earth and in Space, In: Moving Boundaries V (B. Sarler, C.A. Brebbia and H. Power Eds.) WIT Press, Southampton, pp 111-120.

2. Gerrits, J.: 2001, Dynamics of Liquid-Filled Spacecraft, Numerical Simulation of Coupled Solid-Liquid Dynamics, PhD thesis, RuG.

3. Fekken, G., Veldman, A.E.P. and Buchner, B.: 1999, Simulation of Green Water Flow Using the Navier-Stokes Equations, Seventh International Conference on Numerical Ship Hydromechanics, Nantes.

4. Van Daalen, E. F. G., Kleefsman, K. M. T., Gerrits, J., Luth, H.R., Veldman, A.E.P., "Anti Roll Tank Simulations with a Volume of Fluid (VOF) based Navier-Stokes Solver", 23rd Symposium on Naval Hydrodynamics, September 2000, Val de Reuil.

5. Buchner, B., Bunnik, T.H.J., Fekken, G. and Veldman, A.E.P.: 2001, A Numerical Study on Wave Run Up on an FPSO Bow, OMAE2001, Rio de Janeiro.

6. Fekken, G: 2004, Numerical Simulation of green water flow, PhD thesis, RuG

7. Kleefsman, K.M.T., Fekken, G., Veldman, A.E.P., Bunnik, T., Buchner, B. and Iwanowski, B.; "Prediction of green water and wave impact loading using a Navier-Stokes Based Simulation Tool", OMAE conference, Oslo, 2002

8. Buchner, B., Loots, G.E.: 2004, Wave run up as important hydromechanic issue for gravity based structures, OMAE 2004

9. Hirt, C.W. and Nichols, B.D.1981, "Volume Of Fluid (VOF) Method for the Dynamics of Free Boundaries", Journal of Computational Physics, 39, pp 201-225.